Measuring the Charge State of Point Defects on MgO/Ag(001)

T. König,[†] G. H. Simon,[†] H.-P. Rust,[†] G. Pacchioni,[‡] M. Heyde,[*,†] and H.-J. Freund[†]

Fritz-Haber-Institut der Max-Planck-Gesellschaft, Faradayweg 4-6, D-14195 Berlin, Germany, and Dipartimento di Scienza dei Materiali, Università di Milano-Bicocca, via R. Cozzi, 53-20125 Milano, Italy

Received September 30, 2009; E-mail: heyde@fhi-berlin.mpg.de

Electron transfer processes play an important role in chemical reactions in general and in particular in catalysis. Surface defects are crucial in catalysis as oxide surfaces are often present either as supports or directly as catalysts.[1−7] To understand these transfer processes at the atomic level on surfaces, one has to determine the charge state and local position of defect sites present on the surface. A particular simple example is the MgO surface. While the perfect single crystal surface is quite unreactive, a defect rich surface shows a rich and complex chemical reactivity.[8] Here we have measured the local charge state of individual point defects on a MgO/Ag(001) surface, providing identification of electron trapping sites, i.e. F^{2+}, F^+, F^0 centers, and morphological defects like divacancies (DV). F^{2+}, an anion vacancy formed by removing an O^{2-} ion, is positively charged; this center can trap one or two electrons leading to the charged F^+ or to the neutral F^0 centers, respectively. F centers on MgO are deep electron traps. There are also shallow traps on the MgO surface, e.g low-coordinated Mg^{2+} ions at corner sites or divacancies consisting of missing O and Mg neighbors. These neutral sites can bind electrons with energies of 0.6−1 eV forming negative defects on the surface (DV⁻).[9,10] To address the spatial position, electronic signature, and local potential of the defects at the atomic scale, techniques with high lateral resolution are necessary. Both frequency modulated dynamic force microscopy (FM-DFM) and scanning tunneling microscopy (STM) match these requirements. The microscope employed in this study is a dual mode, i.e. a combined FM-DFM/STM setup[11] to utilize the complementary strength of both techniques at the same surface area with the same tip. To achieve a stable operating condition, liquid helium was used to cool the microscope stage to 5 K. To benefit from the local resolution of FM-DFM/STM model systems thin MgO films (3 and 6 monolayers) grown on Ag(001) have been prepared.[12] The presented measurements show the same trends for both film thicknesses. However, FM-DFM is also applicable to bulk insulators and is not limited to thin films. Clean and well grown MgO areas have been selected to ensure defined conditions. The intrinsic defect density of the film is very low. To increase the number of defects available, the scan frame was scanned in the field emission regime at high voltages and currents; typical values are bias voltage $V_S = 7$ V and current $I_T = 6$ nA. The defects are preferentially located at kinks, corners, and step edges. An FM-DFM image of a MgO step edge with point defects is shown in Figure 1a. The detection of the defects is based on the high local resolution of the microscope.

The displacement in z shows a strong peak at the defect's position. These measurements, with point defect resolution, enable local tip positioning above the defect. On the defects' positions the frequency shift with respect to the applied bias voltage has been measured and compared with measurements directly next to the defect. During these measurements the tip height was constant. The frequency shift vs bias voltage curves show a parabolic behavior (see Figure 1b) due to the electrostatic force acting between tip and sample:[13−15]
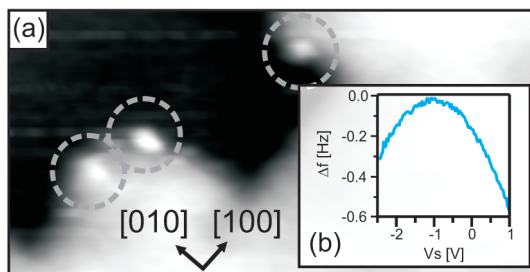

[†] Fritz-Haber-Institut der Max-Planck-Gesellschaft.
[‡] Università di Milano-Bicocca.

Figure 1. (a) FM-DFM image taken at constant Δf showing a MgO step edge with point defects (indicated by the dashed circles). Scan range: 23.0 × 11.5 nm²; $\Delta f = -1.6$ Hz; $V_S = -50$ mV. (b) Presents a typical frequency shift vs bias voltage curve taken on a defect position.

$$F_{el} = \frac{1}{2C_{\Sigma}^2}\frac{\partial C_1}{\partial z}\left(nq + C_2\left(V_S - \frac{\Delta\Phi_{loc}}{|q|}\right)\right)^2 \quad (1)$$

where $C_{\Sigma}(z) = C_1(z) + C_2$, with $C_1(z)$ as the capacity between tip and defect and C_2 as the capacity between defect and substrate. q is the local defect charge while n represents the number of elementary charges. An additional term representing the capacity between the tuning fork's back-electrode and the substrate can be added to eq 1 but is irrelevant for point defect resolution. The electrostatic force is always attractive, i.e. independent of the voltage sign due to the quadratic term. The maximum of the parabola is determined by the charge q and the local potential $\Delta\Phi_{loc}$ (sometimes called local work function). The presence of the MgO overlayers shifts the Ag(001) work function by ~ -1.1 eV.[16,17] This is the reference level. From measurements of numerous defects four different types have been distinguished by the maximum positions of the parabola. Figure 2 shows to the left the four types indicated by numbers and the MgO reference. The graph shows the maximum positions of the parabola with respect to the reference measurement on MgO (bottom abscissa) and with respect to the Ag(001) level (top abscissa).

For a type I defect the shift is −50 and −25 meV below the MgO level. This significant shift is due to a positively charged defect with respect to the surrounding area resulting in a decrease in the local potential (see Figure 2). This shift is assigned to a F^{2+} defect (see assignment (AS) in Figure 2).

Considering defect type II the shift changes its sign and shows a shift of $\sim +9$ meV. The shift is assigned to a F^+ defect. The overall charge is positive, but on the local scale the single electron has a probability density above the surface as derived by density functional calculations.[18] The charge changes the local dipole moment such that the local potential increases compared to the MgO/Ag(001) reference level. For a type III defect the shift is +15 to +20 meV above the MgO level. This shift results from two charges present in a defect site representing a F^0 center. The F^0 is neutral compared to the surrounding MgO lattice, but the two electrons present have a large probability density above the surface due to their Coulomb repulsion.[18] This results in a stronger local dipole moment compared to defect type II, and thus the shift is approximately twice as large as that for type II. Defect
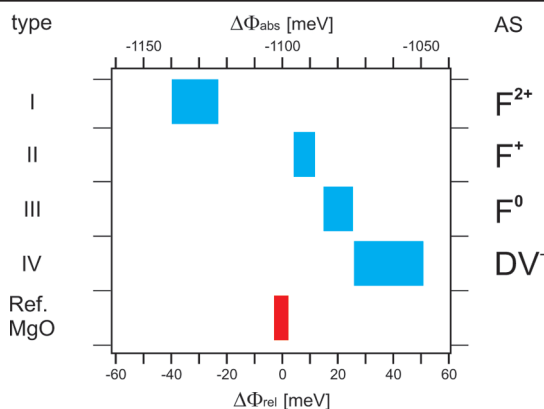
Figure 2. The left labeling assigns the defects to numbers. The graph shows the relative shift of the local potential $\Delta\Phi_{rel}$ with respect to the MgO surface (bottom abscissa) and the absolute shift $\Delta\Phi_{abs}$ with respect to the Ag(001) level (top abscissa), both shifts including the local charge. The covered range in the shifts results from measurements with different local resolutions due to different tip structures. The labeling on the right gives the assignment (AS) of the defect types.
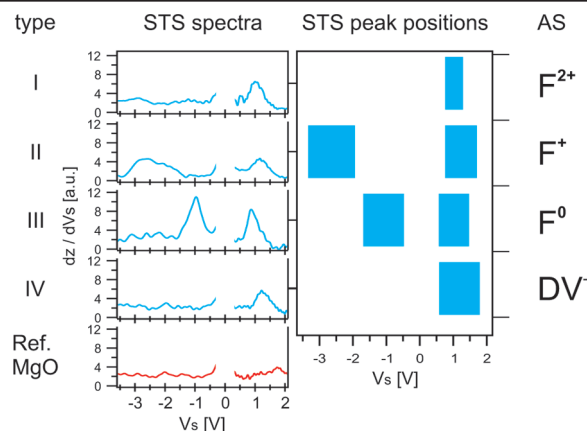

Figure 3. The left label indicates the different defect types by numbers. The left graph shows STS spectra of the respective defect. The right graph presents the maxima of the STS data. The covered abscissa range accounts for the statistics of the peak positions. The identification of defect types with color centers and negatively charged divacancies (DV⁻) according to theory is implemented to the right.

type IV has a positive shift stronger than that of types II and III indicating that negative charges might be involved. Thus this shift can in principle be attributed to divacancies or OH groups trapped at low coordinated Mg^{2+} sites. OH groups are potential electron traps.[19] However, OH groups can be excluded since all defects occur only after high voltage and current imaging and are not present on regular MgO terraces or steps. Favored candidates are divacancies formed at steps or corner sites. The stability of divacancies on the MgO surface and their electron affinity for trapping electrons have been confirmed by DFT calculations.[9] These structural facts in combination with a locally defined negative charge are expected to result in a strong local potential shift as detected. Thus, all analyzed defect types show a characteristic fingerprint due to different charge states.

Additional and supporting measurements for all defect types were performed with scanning tunneling spectroscopy (STS). The electronic signature of the defects, i.e. the local density of states (LDOS) at the defects' positions, has been analyzed complementary by STS directly after the local potential measurements without moving the tip laterally. The defects' spectra are compared to MgO spectra taken on the MgO terrace next to the defect.

The F^{2+} center shows peaks only in the unoccupied regime at voltages of $\sim +1$ V above the Fermi level (Figure 3 left and right graph). The F^+ defect has both occupied and empty electron states located within the band gap of MgO (compare red reference spectrum taken on the bare MgO); the filled states are close to the valence band and occur at voltages between -3.5 to -2.0 V below the Fermi level, depending on the defect location on the film.[3] The empty states are at $\sim +1$ V above the Fermi level. In F^0 the doubly occupied state is higher in energy, ~ -1 V below the Fermi level, while the position of the empty state is similar as in F^+. The last defect, a morphological site (e.g., a divacancy) with a trapped electron, shows only an empty feature at $\sim +1$ V above Fermi level. The corresponding occupied shallow state is expected to be very close to the Fermi level, i.e. in a region where our experiment cannot detect states. Finally, it should be mentioned that F^0 and shallow traps (e.g., divacancies) are equally frequent and represent $\sim85\%$ of the total defects while F^+ centers are much less frequent, $\sim10\%$. Only $\sim5\%$ of all defects are F^{2+} centers. This is fully consistent with the high formation energy of F^{2+} defects.

Four of the major and in literature mostly discussed defect types in MgO have been characterized by their charge state and finally identified by the complementary application of FM-DFM and STM in combination with DFT results.[18] Their preferred edge, kink, and corner sites could be confirmed. STS revealed the defects electronic states located in the band gap of the MgO surface. The characterization of F^0, F^+, F^{2+} and shallow morphological traps like divacancies has been possible by local potential differences arising from different charge states of the defects. For the first time, the rich and complex nature of point defects at the MgO surface is directly observed, a result which can significantly improve our understanding of the chemistry of this as well as of other oxide surfaces.

Supporting Information Available: Details of the setup and additional experimental information. This material is available free of charge via the Internet at http://pubs.acs.org.

References

(1) Sterrer, M.; Fischbach, E.; Risse, T.; Freund, H.-J. *Phys. Rev. Lett.* **2005**, *94*, 186101.
(2) Sterrer, M.; Fischbach, E.; Heyde, M.; Nilius, N.; Rust, H.-P.; Risse, T.; Freund, H.-J. *J. Phys. Chem. B* **2006**, *110*, 8665–8669.
(3) Sterrer, M.; Heyde, M.; Novicki, M.; Nilius, N.; Risse, T.; Rust, H.-P.; Pacchioni, G.; Freund, H.-J. *J. Phys. Chem. B* **2006**, *110*, 46–49.
(4) Neyman, K. M.; Inntam, C.; Matveev, A. V.; Nasluzov, V. A.; Rösch, N. *J. Am. Chem. Soc.* **2005**, *127*, 11652–11660.
(5) Yan, Z.; Chinta, S.; Mohamed, A. A.; Fackler, J. P.; Goodman, D. W. *J. Am. Chem. Soc.* **2005**, *127*, 1604–1605.
(6) Pacchioni, G.; Sicolo, S.; Di Valentin, C.; Chiesa, M.; Giamello, E. *J. Am. Chem. Soc.* **2008**, *130*, 8690–8695.
(7) Trevethan, T.; Shluger, A. *Nanotechnology* **2009**, *20*, 264019.
(8) Pacchioni, G. *Theory of point defects at the MgO surface*; Elsevier Science B.V.: 2001; Chapter 3, pp 94−135.
(9) Ricci, D.; Pacchioni, G.; Shusko, P. V.; Shluger, A. L. *J. Chem. Phys.* **2002**, *117*, 2844–2851.
(10) Sushko, P. V.; Gavartin, J. L.; Shluger, A. L. *J. Phys. Chem. B* **2002**, *106*, 2269–2276.
(11) Heyde, M.; Simon, G. H.; Rust, H.-P.; Freund, H.-J. *Appl. Phys. Lett.* **2006**, *89*, 2263107.
(12) Schintke, S.; Schneider, W.-D. *J. Phys.: Condens. Matter* **2004**, *16*, R49–R81.
(13) Waser, R. *Nanoelectronics and Information Technology, Advanced Electronic Materials and Novel Devices*, 2nd ed.; Wiley: 2005; Chapter 16, pp 426−427.
(14) Stomp, R.; Miyahara, Y.; Schaer, S.; Sun, Q.; Guo, H.; Grütter, P.; Studenikin, S.; Poole, P.; Sachrajda, A. *Phys. Rev. Lett.* **2005**, *94*, 056802.
(15) Gross, L.; Mohn, F.; Liljeroth, P.; Repp, J.; Giessibl, F. J.; Meyer, G. *Science* **2009**, *324*, 1428–1431.
(16) König, T.; Simon, G. H.; Rust, H.-P.; Heyde, M. *J. Phys. Chem. C* **2009**, *113*, 11301–11305.
(17) Giordano, L.; Cinquini, F.; Pacchioni, G. *Phys. Rev. B* **2005**, *73*, 045414.
(18) Giordano, L.; Martinez, U.; Pacchioni, G.; Watkins, M.; Shluger, A. L. *J. Phys. Chem. C* **2008**, *112*, 3857–3865.
(19) Napoli, F.; Chiesa, M.; Giamello, E.; Finazzi, E.; Di Valentin, C.; Pacchioni, G. *J. Am. Chem. Soc.* **2007**, *129*, 10575–10581.

JA908049N